Electrochimica Acta 542 (2025) 147389

Contents lists available at ScienceDirect

Electrochimica Acta

journal homepage: www.journals.elsevier.com/electrochimica-acta

Scaling relations and catalytic descriptor for the nitrogen reduction on single-atom catalysts

Matteo Spotti [a], Kevin Maineri [a], Francesc Viñes [b], Francesc Illas [b], Giovanni Di Liberto [a,*], Gianfranco Pacchioni [a,*]

[a] Department of Materials Science, University of Milano-Bicocca, Via Cozzi 55, Milano 20125, Italy
[b] Departament de Ciència de Materials i Química Física & Institut de Química Teòrica i Computacional (IQTCUB), Universitat de Barcelona, c/ Martí i Franquès 1-11, Barcelona 08028, Spain

ARTICLE INFO

Keywords:
SAC
DFT
NRR

ABSTRACT

Single-atom catalysis is a rapidly advancing frontier in catalysis research, with the electrochemical synthesis of NH_3 from N_2 representing a key transformation. In this study, we conducted a computational investigation of a series of single-atom catalysts (SACs), each composed of a single metal atom anchored on nitrogen-doped graphene, to enhance understanding of their complex chemistry in the nitrogen reduction reaction. The results indicate that the most likely pathway depends on the nature of the metal atom and can differ from the classical pathways found on extended catalytic surfaces. Besides electrochemical intermediates, the formation of molecular adducts such as $*N_2$ and $*NH_3$ cannot be neglected. Interestingly, it is possible to correlate the stability of reaction intermediates via scaling relations with a simple yet practical descriptor, depending on the stability of two species only, *NNH and $*NH_2$. This descriptor enables us to rationalize the volcano-shaped dependence of the nitrogen reduction reaction's rate-limiting step and may serve as a useful proxy for screening large catalyst databases, providing qualitative and semi-quantitative insights for more advanced refinement. Last, we show that the $*N_2$ and $*NH_3$ chemical adsorbates must be explicitly considered in order to reliably predict the catalyst behavior.

1. Introduction

Catalysis plays a pivotal role in our society [1], as the vast majority of commodity chemicals are obtained through catalytic processes involving heterogenous catalysts. A key process is the synthesis of ammonia, which is produced industrially from gas-phase nitrogen and hydrogen via the Haber-Bosch reaction in harsh conditions [2]. Ammonia is at the basis of fertilizers, which in turn are fundamental to substantiate the still growing population on our planet. This process alone requires about 1 % of the total energy involved in our planet and is responsible of about 1 % of the total CO_2 emission, requiring alternative catalyst able to work in mild conditions [3]. Here, the electrochemical reduction of nitrogen to ammonia is a promising possibility [4].

Several studies have been published over the last years, demonstrating the potential of the nitrogen reduction reaction (NRR) process, highlighting critical aspects, and future directions. The first evidence of electrosynthesis of NH_3 is appointable to Davy back in 1807 [5]. In 2000 Nørskov and co-workers provided seminal evidence with quantum chemical simulations of the synthesis of ammonia below 100 °C using aqueous electrolyte [6]. In recent years, a considerable amount of work has been published devoted to the design of efficient catalysts for ammonia production [7–9]. It is important to underline that the quantitative measurement of ammonia produced is a delicate point [10] as it requires complicated procedures, as those proposed by Greenlee et al. and Li et al. [11,12].

The electrochemical NRR is a complex problem to control, as the N_2 molecule is hard to activate. Also, the most promising catalytic materials are often noble and critical metals, raising questions on the overall sustainability of the process. The process is also competitive with the hydrogen evolution reaction (HER), implying that the catalyst should be selective for NRR rather than to water splitting [13–15].

Computational chemistry is a valuable and useful approach to provide an atomistic description of the chemistry behind this process. For instance, it is possible to search for catalytic descriptors, i.e. physicochemical properties allowing to provide a measure of the predicted activity of a material [16,17]. Several papers have been proposed over the

* Corresponding authors.
E-mail addresses: giovanni.diliberto@unimib.it (G. Di Liberto), gianfranco.pacchioni@unimib.it (G. Pacchioni).

https://doi.org/10.1016/j.electacta.2025.147389
Received 23 July 2025; Received in revised form 11 September 2025; Accepted 14 September 2025
Available online 15 September 2025
0013-4686/© 2025 The Author(s). Published by Elsevier Ltd. This is an open access article under the CC BY license (http://creativecommons.org/licenses/by/4.0/).

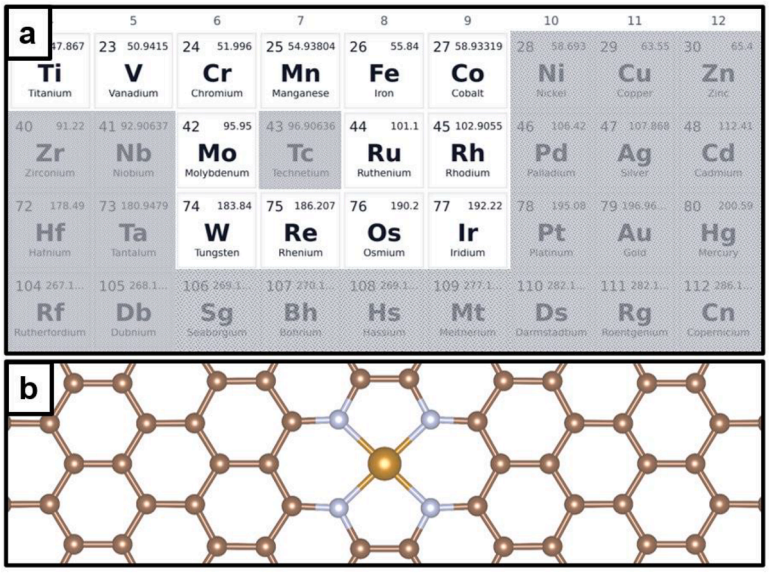

Fig. 1. (a) Transition metals investigated, Ti, V, Cr, Mn, Fe, Co, Mo, Ru, Rh, W, *Re*, Os, Ir. (b) Top view of the TM@4N-Gr structure. C, metal, and N atoms are shown as brown, golden, and light blue spheres, respectively.

past years, showing that the activity scales with the stability of key reaction intermediates. Skúlason et al. demonstrated that activation energy barriers scale with adsorption Gibbs free energies, identifying Mo, Fe, Rh, and Ru as active transition metals for NRR [18]. Nørskov and co-workers showed that in this complex picture, the ability of the catalyst to bind the first electrochemical reaction intermediates, *NNH, and the intermediate preceding the release of ammonia, $*NH_2$, play a critical role [19]. The crucial role of *NNH formation was discussed also in other works [20–22].

A promising frontier to reduce the amount of noble metal loading and promote the activation of nitrogen is represented by single-atom catalysts (SACs) [23–29], which can be viewed as solid-state analogues of coordination chemistry compounds [30–34]. This is at the basis of their nature, bridging the two classical worlds of homogeneous and heterogenous catalysis [35,36]. Eventually, both the nature of the metal and its local coordination determine the reactivity of the system [37–39]. This complex chemistry makes the search for general rules governing their stability, nature, and reactivity particularly challenging.

In this work we drew insight from papers devoted to NRR in heterogeneous catalysis and investigated the existence of scaling relations on SACs, with the aim of identifying a simple yet practical catalytic descriptor. To this end, we considered a set of SACs made by 13 transition metal atoms anchored in a pyridinic defect of nitrogen-doped graphene, a widely investigated model system [40–43], Fig. 1. In this context, it is important to note that the goal of the study is not to provide absolute predictions, but rather to convey a general understanding of the correlation between the predicted activity and reactivity of the SACs. Even at this level it is essential to add a series of key-ingredients to the classical framework used to model heterogenous catalysts [44,45]. The results of our study show that new scaling relations can be extracted for the NRR. Of course, this is not the first time that simple descriptors have been proposed to predict the activity of a SAC in the NRR. For instance, by combining the intrinsic physical properties of the metal atom with those of its coordinated atoms, sets of descriptors have been suggested for SACs stabilized on $B_3C_2P_3$ [46], C_2N-based monolayers [47], and BN nanosheets [48], among others.

There are two important novel aspects in our work: (1) the predicted catalytic activity can be rationalized in terms of a descriptor determined by the balance between the ability of SACs to bind the *NNH and $*NH_2$ intermediates; (2) we provide evidence that it is not possible to exclude from the simulation protocol the formation of molecular complexes, such as $*N_2$ and $*NH_3$. This is an important aspect, as the formation of $*N_2$, and especially $*NH_3$ are often overlooked. This study lays the foundation for future research focused on designing SACs with optimized binding affinity for key intermediates. Despite the very complex chemistry behind NRR on SACs, the results of the study provide evidence of the existence of simple relations allowing one to correlate stability of intermediates with catalytic activity, which could be used as proxy for screening studies followed by more elaborated and dedicate investigation on promising candidates.

2. Computational details

We performed spin-polarized density functional theory (DFT) calculations as implemented in the *Vienna Ab-initio* Simulation package (VASP) [49–51]. The Perdew-Burke-Ernzherof (PBE) exchange and correlation functional was adopted [52]. The effect of core electrons on the valence electron density was accounted for by means of the projector augmented wave (PAW) method [53,54], which is essentially a frozen core all electron approach. The valence electrons density was expanded on a plane waves basis set with a kinetic cutoff equal to 400 eV. The threshold criteria for electronic and geometry loops were set to 10^{-5} eV and 10^{-2} eV/Å respectively. A $2 \times 2 \times 1$ Monkhorst−Pack k-point grid [55] was used to sample the reciprocal space. The Grimme's D3 parametrization scheme was adopted to account for dispersion interactions [56]. Geometry optimizations were performed by means of the conjugate gradient algorithm.

Metal atoms in SACs can retains a residual spin density due to the reminiscence of atomic-like character [57]. This implies the usage of functionals accounting, at least in part, for the self-interaction, as in hybrid functionals. In fact, accurate comparisons of DFT and coupled cluster calculations for TM complexes have shown that hybrid functionals are required in order to obtain accurate descriptions of the adsorption energies, in particular for systems with open shell ground states [58]. A strategy to reduce the large increase of the computational cost involved in the calculations with hybrid functionals when a plane wave basis set is used, without any relevant loss of accuracy, is to perform single-point calculations with hybrid functionals on-top of PBE optimized structures. This strategy improves the description of the electronic structure [59–62], as is the one adopted here by using the PBE0 functional [63].

We started from a graphene nanosheet and created a (4 × 4)

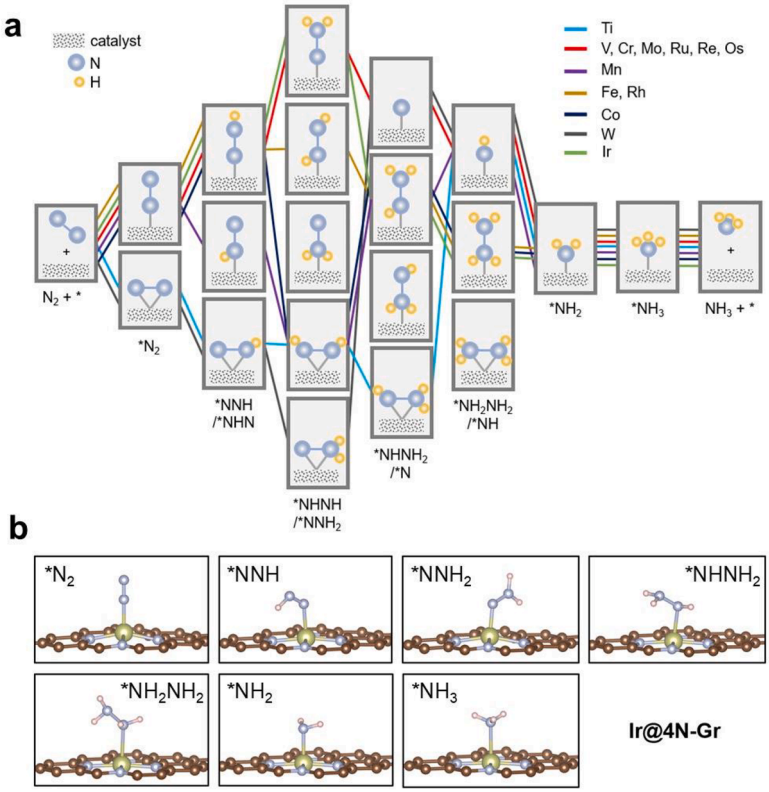

Fig. 2. (a) Schematic NRR pathways on a SAC. (b) Example of the most stable intermediates on Ir@4N-Gr. Color coding as in Fig. 1, while H atoms are shown as white spheres.

supercell, with lattice parameters a and b equal to 9.870 Å, and $\gamma = 120^{\circ}$ A carbon divacancy was created and four carbon atoms were replacing by nitrogen ones. The metal was hosted in the resulting cavity. In all cases, the atomic coordinates were fully relaxed. A vacuum layer of 15 Å was added to avoid spurious effects due to interaction between periodic replicas of the system. The cartesian coordinates of the 4N-Gr model are reported in the SI.

The NRR was modelled by using the computational hydrogen electrode (CHE) approach [64,65]. The Gibbs free energy ΔG_x of a given reaction intermediate x is obtained by adding entropic ΔS_x and zero-point energy $\Delta E_{zpe,x}$ contributions to the calculated DFT reaction energy, ΔE_x. Zero-point energies (ZPE) were calculated within the harmonic approximation by allowing displacements of the metal atoms and those of the intermediates. Entropy of solid-state species was approximated from the vibrational partition function of the adsorbed intermediates calculated from Equation S1 [66], whereas that of gas-phase species was taken from thermodynamic tables. We neglected any reaction barriers different from those arising purely from the thermodynamic profile. The calculated working quantities are reported in Table S1. Gibbs free energy profiles were calculated assuming to work at the reaction equilibrium potential ($V_{N2/NH3} = -0.16$ V).

In this work we neglected solvent effects despite the fact that solvents can play an active role in SAC reactivity, often acting as ligands rather than serving solely to solvate [67]. In two selected cases, Fe@4N-Gr and Co@4N-Gr, an implicit solvent model has been used to recompute the free energies of formation of the various intermediates, but the changes are of the order of 0.1–0.2 eV, see Table S2 and Fig. S1. A fully quantitative description of electrochemical systems would require explicit solvent modelling alongside other factors such as electrolyte composition, applied potential, and pH, each of which significantly influences the final results. Such complexity lies beyond the scope of the present work. Here, our goal is to use simplified models to identify descriptors that capture the main trends and enable efficient screening of new catalysts.

3. Results and discussion

3.1. Reaction intermediates and pathways

We studied the behaviour of the SACs reported in Fig. 1. They consist of transition metal atoms (TM = Ti, V, Cr, Mn, Fe, Co, Mo, Ru, Rh, W, *Re*, Os, Ir) embedded in the fourfold cavity of nitrogen-doped graphene, and the resulting system is hereafter referred to as TM@4N-Gr. We have also considered the group of Ni, Pd, Pt, but we observed that they are not able to bind N_2. Therefore, they will not be further discussed.

At variance with the classical thermal catalysis process, where in the first reaction step N_2 is dissociated into two nitrogen atoms, 2N*, in the NRR the process proceeds through a series of coupled electron-proton transfer steps [68]. However, when dealing with SACs, one needs to consider the formation of molecular adsorbed complexes as well, such as *N_2 and *NH_3. In the case of N_2, two adsorption configurations are possible: end-on (η^1) and side-on (η^2).

Two possible pathways are considered for the reaction. In the *distal* mechanism, coupled proton-electron transfer steps primarily occur on one (terminal) nitrogen atom of the adsorbed N_2 molecule, leading to its full reduction and then to the release of one NH_3 molecule, followed by the reduction of the other nitrogen atom on the surface (N*), releasing the second NH_3 molecule. Conversely, in the *alternating* mechanism, coupled proton-electron transfer steps occur successively on both the distal and proximal nitrogen atoms of the adsorbed N_2 molecule. Alternative pathways, called *enzymatic* and *consecutive*, can be obtained having the nitrogen atom η^2 coordinated to the catalyst [69].

In this work the analysis goes beyond the conventional mechanisms, as SACs can form unconventional reaction intermediates breaking classical pathways [70,71]. The reaction was modelled by considering the formation of all possible reaction intermediates, as depicted in

Table 1
Adsorption energy, TM-N and N—N bond distances, TM-N-N bond angle of $*N_2$ adsorbed on TM@4N-Gr and Bader charge analysis of TM and N_2.

Metals	ΔE /eV	d(TM-N) /Å	d(N—N) /Å	θ(TM-N-N) /°	Δq (TM)	q(N_2)
Ti	−0.93	2.09	1.19	74.4	0.24	−0.61
V	−0.86	1.92	1.15	179.9	0.17	−0.35
Cr	0.54	1.86	1.14	180.0	0.25	−0.28
Mn	0.80	1.77	1.14	180.0	−0.02	−0.29
Fe	0.45	1.75	1.14	180.0	0.00	−0.17
Co	0.09	1.85	1.13	180.0	0.07	−0.09
Mo	−0.86	1.96	1.15	180.0	0.35	−0.41
Ru	−0.80	1.85	1.14	180.0	0.10	−0.26
Rh	0.29	2.03	1.13	180.0	0.29	−0.15
W	−1.46	1.94	1.30	70.4	0.26	−0.95
Re	−0.67	1.91	1.15	179.3	0.05	−0.35
Os	−1.06	1.85	1.15	180.0	0.29	−0.35
Ir	0.39	1.94	1.14	180.0	0.33	−0.18

Table 2
Adsorption energy, TM-N bond distance and TM-N-N bond angle of $*NH_3$ on TM@4N-Gr.

Metals	ΔE /eV	d(TM-N) /Å	θ(TM-N-H) /°
Ti	−2.52	2.22	109.7
V	−2.19	2.14	110.7
Cr	−1.10	2.17	110.9
Mn	−0.55	2.33	109.9
Fe	−0.75	1.96	110.5
Co	−1.61	2.18	110.0
Mo	−1.95	2.29	107.5
Ru	−3.63	2.06	110.5
Rh	−1.59	2.36	109.6
W	−4.79	2.27	108.9
Re	−1.53	2.19	110.4
Os	−3.63	2.14	111.5
Ir	−1.32	2.36	109.99

Fig. 2a. The preferred pathway is defined by the most stable reaction intermediates for a given number of coupled proton-electron steps. Fig. 2b shows Ir@4N-Gr as an illustrative example. All elementary steps that can occur on the reaction are reported in Eq. 1–19.

(1) $N_2 + * \rightarrow *N_2$
(2) $*N_2 + H^+ + e \rightarrow *NNH$

Table 3
Calculated maximum thermodynamic Gibbs free energy change (h_{max}) of NRR on TM@4N-Gr.

	TM	h_{max} /eV	Step
Electrochemical intermediates only	Ti	3.27	$*NH_2 \rightarrow NH_3$
	V	2.58	$*NH_2 \rightarrow NH_3$
	Cr	2.27	$N_2 \rightarrow *NNH$
	Mn	2.49	$N_2 \rightarrow *NNH$
	Fe	2.50	$N_2 \rightarrow *NNH$
	Co	2.29	$N_2 \rightarrow *NNH$
	Mo	2.51	$*NH_2 \rightarrow NH_3$
	Ru	2.92	$*NH_2 \rightarrow NH_3$
	Rh	1.56	$N_2 \rightarrow *NNH$
	W	3.30	$*NH_2 \rightarrow NH_3$
	Re	2.26	$*NH_2 \rightarrow NH_3$
	Os	3.36	$*NH_2 \rightarrow NH_3$
	Ir	1.48	$N_2 \rightarrow *NNH$
All intermediates pathway	Ti	2.52	$*NH_3 \rightarrow NH_3$
	V	2.19	$*NH_3 \rightarrow NH_3$
	Cr	1.20	$*N_2 \rightarrow *NNH$
	Mn	1.35	$N_2 \rightarrow *N_2$
	Fe	1.49	$*N_2 \rightarrow *NNH$
	Co	1.68	$*N_2 \rightarrow *NNH$
	Mo	1.95	$*NH_3 \rightarrow NH_3$
	Ru	3.63	$*NH_3 \rightarrow NH_3$
	Rh	1.59	$*NH_3 \rightarrow NH_3$
	W	4.79	$*NH_3 \rightarrow NH_3$
	Re	1.53	$*NH_3 \rightarrow NH_3$
	Os	3.63	$*NH_3 \rightarrow NH_3$
	Ir	1.32	$*NH_3 \rightarrow NH_3$

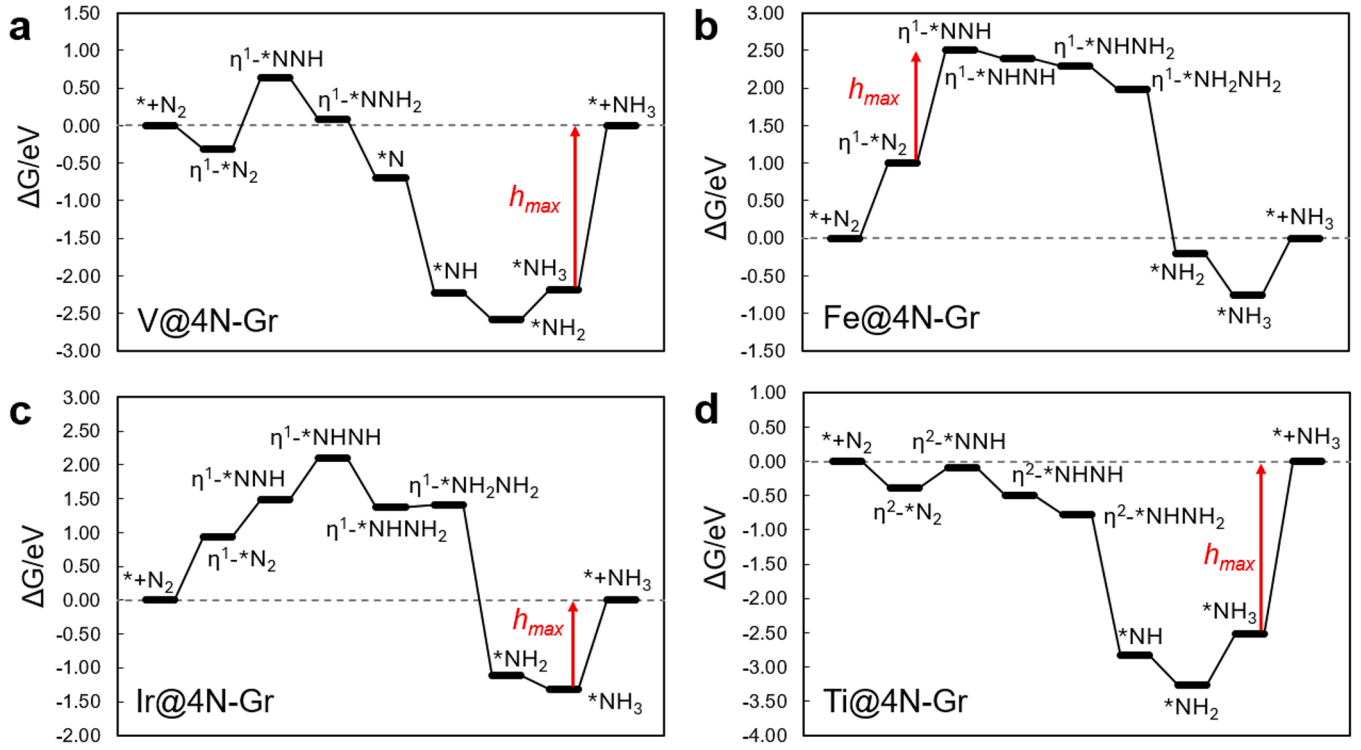

Fig. 3. Selected Gibbs free energy profiles of NRR on: (a) V@4N-Gr; (b)Fe@4N-Gr; (c) Ir@4N-Gr; (d) Ti@4N-Gr. Free energy profiles are calculated at the equilibrium potential of the reaction ($V_{N2/NH3} = -0.16$ V).

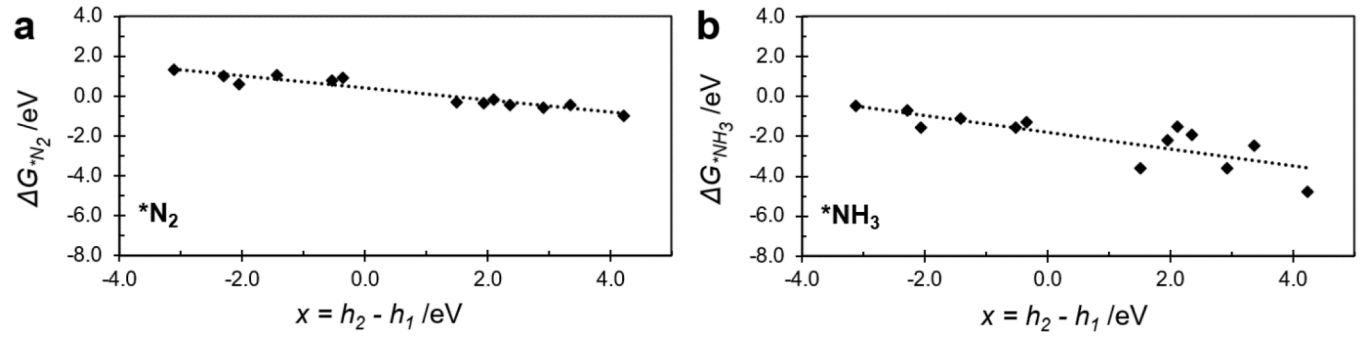

Fig. 4. Scaling relationships between the proposed descriptor $x = h_2 - h_1$ and adsorption Gibbs free energy of (a) $*N_2$ and (b) $*NH_3$.

(3) $*N_2 + H^+ + e^- \rightarrow *NHN$
(4) $*NNH + H^+ + e^- \rightarrow *NHNH$
(5) $*NNH + H^+ + e^- \rightarrow *NNH_2$
(6) $*NHN + H^+ + e^- \rightarrow *NHNH$
(7) $*NHN + H^+ + e^- \rightarrow *NH_2N$
(8) $*NNH_2 + H^+ + e^- \rightarrow *N + NH_3$
(9) $*NNH_2 + H^+ + e^- \rightarrow *NHNH_2$
(10) $*NHNH + H^+ + e^- \rightarrow *NHNH_2$
(11) $*NH_2N + H^+ + e^- \rightarrow *NH_2NH$
(12) $*N + H^+ + e^- \rightarrow *NH$
(13) $*NHNH_2 + H^+ + e^- \rightarrow *NH_2NH_2$
(14) $*NHNH_2 + H^+ + e^- \rightarrow *NH + NH_3$
(15) $*NH_2NH + H^+ + e^- \rightarrow *NH_2NH_2$
(16) $*NH + H^+ + e^- \rightarrow *NH_2$
(17) $*NH_2NH_2 + H^+ + e^- \rightarrow *NH_2 + NH_3$
(18) $*NH_2 + H^+ + e^- \rightarrow *NH_3$
(19) $*NH_3 \rightarrow NH_3 + *$

The adsorption of $*N_2$ (Eq. 1) represents the initial step of the reaction, where molecular nitrogen is activated through its interaction with the metal single-atom site. All catalysts in the studied database exhibit mild activation of the nitrogen molecule, with the N–N bond length increasing from the reference value 1.11 Å (isolated N_2) to 1.13–1.30 Å upon adsorption, Table 1. Ti and W lead to η^2-$*N_2$, all the rest of TMs lead to η^1-$*N_2$. In the case of η^1-$*N_2$, the adduct shows a TM-N-N bond angle close to 180°, Table 1. When $*N_2$ assumes a η^2 configuration, it results in a more pronounced bond length elongation. A qualitative correlation can be established between the adsorption energy and the N–N bond length: the weaker the interaction between the molecule and the catalyst, the shorter the N–N bond, Table 1. The adsorption of N_2 to the catalyst can induce an elongation of the N—N bond, which is a proxy of its activation. Another important quantity is the adsorption energy. In our SACs, the adsorption energies range from −1.46 eV (W@4N-Gr) to 0.80 eV (Mn@4N-Gr). W@4N-Gr is a peculiar case, as N_2 is strongly adsorbed to the SAC, and the analysis of atomic charges suggests that a charge transfer occurs forming a N_2^- like species. The adsorption energy is also comparable with previous studies of N_2 adsorption on other catalytic materials [72], where N_2 becomes strongly activated after adsorption.

Notice that, in some cases, the adsorption energy of $*N_2$ is positive, indicating that this state is higher in energy than physisorbed N_2 (ΔE of about −0.1 eV). We underline that the search for scaling relations requires to compare the stability of adducts chemically adsorbed to the catalytic active phase, and for this reason we always used chemisorbed species for the analysis reported below.

The analysis of atomic charges has been performed according to the Quantum Theory of Atoms In Molecules (QTAIM) [73]. Although electronic counting in solids is not quantitative in general [74] it can provide useful information to understand the chemistry behind several chemical processes, including N_2 activation [75]. The analysis of the atomic charges, Table 1, reveals an electron accumulation or polarization towards the $*N_2$ species, with $q(N_2)$ ranging between −0.2 |e| and −0.4 |e|. An exception is observed for Ti and W which exhibit a more pronounced charge transfer toward N_2.

$*NH_3$ desorption represents the final step of the reaction (Eq. 19), in which the product is released from the catalytic site to the gas-phase. The adducts show a bond angle (θ) in the range $107.5° < \theta < 111.5°$, with only small changes with respect to the ideal value for tetrahedral-like complexes. In this context, a strong interaction between ammonia and the single-atom metal centers is evident, with adsorption energies ranging from –0.55 eV to –4.79 eV, Table 2. It is important to note that, according to the Sabatier principle, the desorption step is just as critical as the adsorption ones; too strong binding of the product to the metal can lead to catalyst poisoning, inhibiting its activity.

The calculated adsorption Gibbs free energies of all intermediates are reported in Table S4 whereas Gibbs free energy profiles are reported in Figs. S2-S14; the adsorption configuration of all reaction intermediates is given in Figs. S15-S27. All Gibbs free energy profiles are calculated at the equilibrium potential of the reaction ($V_{N2/NH3} = -0.16$ V).

The most common pathway in our set of catalyst models is the *distal* mechanism, as appears for V@4N-Gr, Cr@4N-Gr, Mo@4N-Gr, Ru@4N-Gr, *Re*@4N-Gr and Os@4N-Gr, Fig. 3a. Systems like Fe@4N-Gr and Rh@4N-Gr follow the *alternating* path, Fig. 3b Interestingly, there are systems following less conventional pathways. For instance, Ir@4N-Gr starts with *distal* mechanism and proceeds the reaction in an *alternating* like pathway, where $*NHNH_2$ is more stable than $*N + NH_3$. Fig. 3c. Ti@4N-Gr starts with an *enzymatic* type reaction, i.e. forming η^2-$*N_2$, and then moves to a *consecutive* path, Fig. 3dW@4N-Gr follows the *consecutive* pathway. Other systems, like Mn@4N-Gr and Co@4N-Gr, form both η^1 and η^2 adducts.

Not surprisingly, NRR is an energy demanding process as the highest thermodynamic Gibbs free energy change (h_{max}) is always larger than 1 eV, Table 3. Considering the most general pathway, which includes the formation of $*N_2$ and $*NH_3$ intermediates, the lowest values of h_{max} are found for Cr, Ir, Mn and Fe with values equal to 1.20 eV, 1.32 eV, 1.35 eV and 1.49 eV, respectively. Recently, it was suggested that a possible way to increase the ability of the catalyst to activate the reaction is to move from single-atom to dual-atom sites, [76] because of the possibility to bind N_2 in a bidentate mode [76–78]. Interestingly, the reaction step associated with h_{max} is always either the formation of *NNH from $*N_2$, or the release of NH_3 from $*NH_3$. The only exception is Mn@4N-Gr where h_{max} is associated to the formation of $*N_2$. When *NNH formation is involved, the catalysts bind too weakly the reaction intermediates, Fig. 3b Mn@4N-Gr is an extreme situation, as the catalyst binds N_2 too weakly. In the case of ammonia desorption, $*NH_3$ step, the SACs are so reactive that the release of the reaction product becomes energetically less favourable, Figs. 3a,c,d

It is important to underline that neglecting the formation of chemical adsorbates, $*N_2$ and $*NH_3$, affects both qualitatively and quantitatively the predictions, Table 3. In fact, in most cases, the value of h_{max} shows sizeable changes. Not surprisingly, this result confirms the importance of including molecular complexes in the theoretical treatment of the

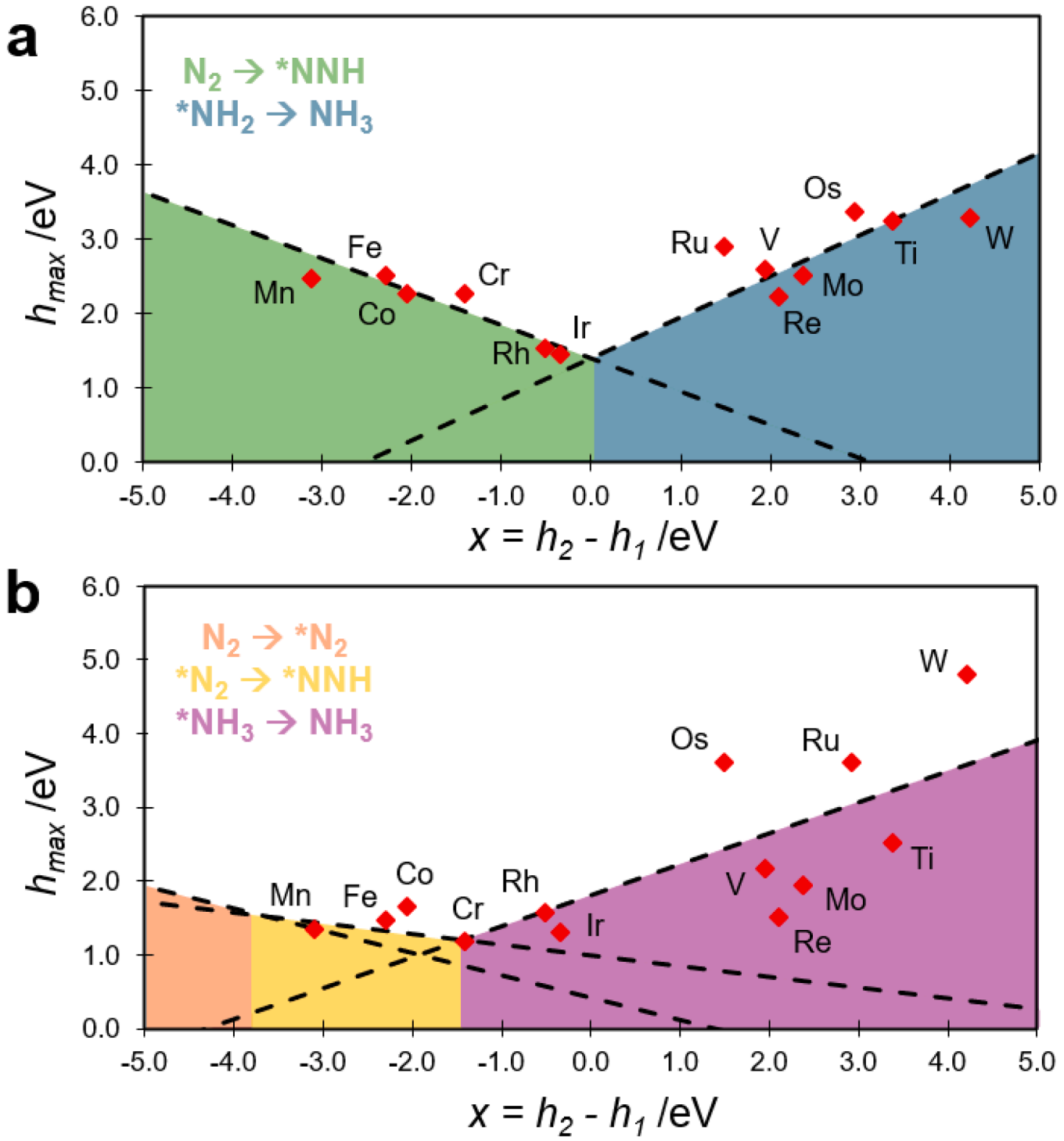

Fig. 5. Calculated h_{max} vs the descriptor $x = h_2 - h_1$ for reaction pathways considering only electrochemical intermediates (a) and both chemical and electrochemical intermediates (b). Different colors correspond to the formation of different intermediates.

reactivity of SACs [76,79,80]. Nevertheless, *NNH or *NH_2 intermediates are still relevant in the reaction steps with the highest energy barrier.

The qualitative analysis of reaction pathways and Gibbs free energy profiles highlights the complexity of formulating general rules to rationalize the reactivity of SACs in the NRR.

3.2. Scaling relations and catalytic descriptors

We now investigate the possibility to correlate the stability of different intermediates. We used a descriptor accounting for the stability of both *NNH and *NH_2 species, due to their recognized importance to describe the reaction on classical heterogenous catalysts. Also, these two species must necessarily form during the reaction. This makes them suitable candidates for describing the activity of SACs. The descriptor at the equilibrium potential of the reaction ($V_{N2/NH3} = -0.16$ V) is defined as $x = h_2 - h_1$, where h_2 is the thermodynamic energy to pass from *NH_2 to NH_3, i.e. $h_2 = -\Delta G_{*NH2} - 0.5\Delta G_{H2}$, and h_1 is the energy to pass from N_2 to *NNH, i.e. $h_1 = \Delta G_{*NNH} - 0.5\Delta G_{H2}$. Fig. S28 shows that the stability of all electrochemical reaction intermediates correlates with the

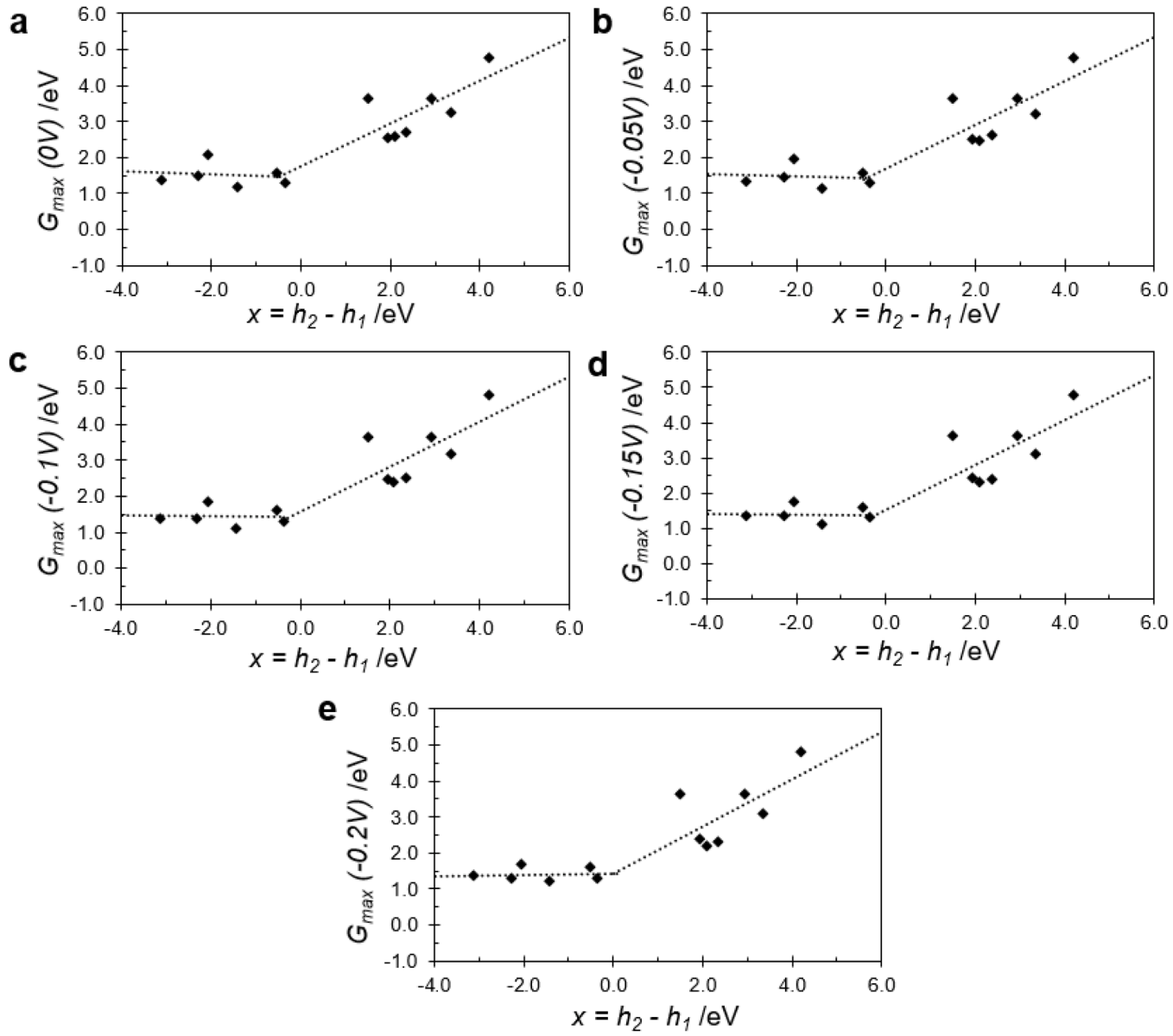

Fig. 6. Calculated $G_{max}(\eta)$ vs. descriptor (x) at 0.0 V (panel a), −0.05 V (panel b), −0.10 V (panel c), −0.15 V (panel d) and −0.20 (panel e).

descriptor $x = h_2 - h_1$ with a linear behaviour. Interestingly, also the Gibbs free energies of adsorption for *N₂ and *NH₃ exhibit a linear scaling relationship with the proposed descriptor, Fig. 4. Table S5 reports the fitted values. This indicates that a descriptor involving only two electrochemical intermediates can correlate also with the stability of purely chemical intermediates.

The existence of scaling relations is in line with previous studies on SACs for other reactions showing that it is still possible to retrieve correlations between the stability of intermediates [81]. Overall, h_{max} scales with the x descriptor in a volcano-like shape, Figs. 5a and 5b, where we can clearly recognize different branches. If we consider only the electrochemical intermediates the first branch describes a regime where the catalyst is too reactive, and the desorption of the product is the rate limiting step. On the other hand, the other branch is associated to values of the descriptor where the formation of *NNH is the limiting step. In this more simplified picture, Fig. 5a, the volcano assumes a symmetric shape and the optimum is found where the Gibbs free adsorption energy of the *NNH and $*NH_2$ species is balanced, according to the Sabatier principle; the SAC should bind both species neither too strongly nor too weakly.

The picture becomes more complex if the formation of $*N_2$ and $*NH_3$ is explicitly considered, Fig. 5b In this case, three distinct branches are observed. The first one corresponds to the adsorption of molecular nitrogen to form *N₂ (Eq. 1); the second one to the subsequent formation of *NNH from *N₂ (Eq. 2); the third one to the desorption of ammonia from *NH₃ (Eq. 19). The resulting volcano plot becomes more asymmetric, with the optimum condition close to a situation where the catalyst is not poisoned by *NH₃, and the limiting step is the formation of *NNH.

Finally, an important quantity in computational electrocatalysis is the limiting potential (U_L), i.e. the minimum value of the applied potential to have all reactions steps downhill in energy. Given this requirement, we considered only electrochemical steps, because the free energy of chemical adducts such as $*N_2$ and $*NH_3$ is not potential dependent in CHE. Interestingly, the proposed descriptor x allows to rationalize qualitatively the trend of U_L, where a volcano like plot is obtained, Figure S29.

Notably, the proposed descriptor is also applicable to SACs in which the *NNH and $*NH_2$ intermediates are not the rate-limiting step in the overall reaction profile. It is important to emphasize that x depends

solely on the stability of two species, while the simulation of the Gibbs free energy profile implies the investigation of a much larger set of intermediates, Fig. 2. Therefore, calculating x is significantly simpler than generating a full Gibbs free energy profile, making it a suitable proxy for screening studies aimed at providing qualitative or semi-quantitative estimates and identifying a subset of promising systems for further investigation.

Finally, we used the span model proposed by Exner [17] to check if the descriptor x correlates with the maximum energy span. The span model was originally developed to provide insights to the description of the Oxygen Evolution Reaction (OER) [82]. Later it was applied also to other problems, such as reaction kinetics of N_2O reduction to N_2 on a MXene catalyst [83]. To the best of our knowledge this is the first application to NRR on SACs. In the span model, one can calculate the maximum free energy change among all possible processes at a given potential (η), $G_{max}(\eta)$ [17]. Exner suggested and detailed that it is possible to correlate G_{max} with kinetic barriers, i.e. to introduce in an approximate way kinetic effects from ab-initio thermodynamics [17]. We calculated G_{max} at small overpotentials going from 0.0 V to 0.20 V, which represents a typical value for this kind of studies [84–87]. Interestingly, $G_{max}(\eta)$ correlates linearly with x, Fig. 6.

4. Conclusions

In this study, we performed a DFT investigation of SACs for the electrochemical reduction of nitrogen to ammonia (NRR), focusing on 13 transition metals (Ti, V, Cr, Mn, Fe, Co, Mo, Ru, Rh, W, *Re*, Os, Ir) embedded in nitrogen-doped graphene. Our analysis of the reaction pathways revealed that the most stable route depends strongly on the nature of the metal and can differ significantly from classical profiles observed on extended surfaces.

By computing the Gibbs free energies of key intermediates, we identified correlations in their stabilities and showed that the formation of molecular adducts, such as $*N_2$ and $*NH_3$, plays a critical role and cannot be neglected, as it affects both the predicted activity and selectivity of the catalysts. Remarkably, we found that the adsorption free energies of $*N_2$ and $*NH_3$ scale linearly with a simple, practical descriptor based on the stability of two key intermediates, *NNH and $*NH_2$. Notice that this holds true also for reactions profiles where the formation of *NNH and the desorption of NH_3 from $*NH_2$ does not correspond to the rate determining step.

The analysis of the thermodynamically limiting steps revealed a volcano-type relationship with the descriptor, with the optimum achieved when the catalyst binds $*NH_3$ moderately, making *NNH formation from $*N_2$ the rate-limiting step. These insights not only enhance our understanding of the chemistry of SACs for NRR but also provide a simple and practical descriptor that can guide the rapid screening of large sets of single-atom catalytic materials and inform more detailed computational or experimental investigations.

Further work will be devoted to the extension of the investigation to other relevant and important class of supporting materials.

Supporting information

Working equations to compute Gibbs free energies of reaction intermediates; Calculated Gibbs free energies of all species and resulting free energy diagrams.

Author information

Matteo Spotti (MS), Dipartimento di Scienza dei Materiali, Università di Milano-Bicocca.

Kevin Maineri (KM), Dipartimento di Scienza dei Materiali, Università di Milano-Bicocca.

Francesc Viñes (FV), Departament de Ciència de Materials i Química Física and Institut de Química Teòrica i Computacional (IQTCUB), Universitat de Barcelona, c/Martí i Franquès 1, 08,028 Barcelona, Spain;

Francesc Illas (FI), Departament de Ciència de Materials i Química Física and Institut de Química Teòrica i Computacional (IQTCUB), Universitat de Barcelona, c/Martí i Franquès 1, 08,028 Barcelona, Spain;/ MS and KM equally contributed to this work.

CRediT authorship contribution statement

Matteo Spotti: Validation, Formal analysis, Data curation. **Kevin Maineri:** Formal analysis, Data curation. **Francesc Viñes:** Writing – review & editing, Supervision. **Francesc Illas:** Writing – review & editing, Conceptualization. **Giovanni Di Liberto:** Writing – original draft, Supervision, Conceptualization. **Gianfranco Pacchioni:** Writing – review & editing, Conceptualization.

Declaration of competing interest

The authors declare no conflict of interest.

Acknowledgements

GDL has received funding through the PRIN project "SACtoH2″ (project code P2022AZETB by the Italian Ministry for Universities and Research (MUR), in the context of the National Recovery and Resilience Plan and co-financed by the European Commission - Next Generation EU (Mission 4, Component 1). Access to the CINECA supercomputing resources was granted via ISCRAB.

Supplementary materials

Supplementary material associated with this article can be found, in the online version, at doi:10.1016/j.electacta.2025.147389.

Data availability

Data will be made available on request.

References

[1] G. Centi, J. Čejka, Needs and gaps for catalysis in addressing transitions in chemistry and energy from a sustainability perspective, ChemSusChem. 12 (2019) 621–632, https://doi.org/10.1002/cssc.201802637.
[2] F. Haber, R.Le Rossignol, The production of synthetic Ammonia, J. Ind. Eng. Chem. 5 (1913) 328–331, https://doi.org/10.1021/ie50052a022.
[3] M. Capdevila-Cortada, Electrifying the Haber–Bosch, Nat. Catal. 2 (2019), https://doi.org/10.1038/s41929-019-0414-4, 1055–1055.
[4] V. Kyriakou, I. Garagounis, A. Vourros, E. Vasileiou, M. Stoukides, An electrochemical Haber-Bosch process, Joule 4 (2020) 142–158, https://doi.org/10.1016/j.joule.2019.10.006.
[5] I. The Bakerian Lecture, on some chemical agencies of electricity, Philos. Trans. R. Soc. Lond. (1807) 97, https://doi.org/10.1098/rstl.1807.0001.
[6] T.H. Rod, A. Logadottir, J.K. Nørskov, Ammonia synthesis at low temperatures, J. Chem. Phys. 112 (2000), https://doi.org/10.1063/1.481103.
[7] Z. Geng, Y. Liu, X. Kong, P. Li, K. Li, Z. Liu, J. Du, M. Shu, R. Si, J. Zeng, Achieving a record-high yield rate of 120.9 μgNH3mgcat.−1h−1 for N2 electrochemical reduction over Ru single-atom catalysts, Adv. Mater. 30 (2018), https://doi.org/10.1002/adma.201803498.
[8] Y.C. Hao, Y. Guo, L.W. Chen, M. Shu, X.Y. Wang, T.A. Bu, W.Y. Gao, N. Zhang, X. Su, X. Feng, J.W. Zhou, B. Wang, C.W. Hu, A.X. Yin, R. Si, Y.W. Zhang, C.H. Yan, Promoting nitrogen electroreduction to ammonia with bismuth nanocrystals and potassium cations in water, Nat. Catal. 2 (2019), https://doi.org/10.1038/s41929-019-0241-7.
[9] H.L. Du, M. Chatti, R.Y. Hodgetts, P.V. Cherepanov, C.K. Nguyen, K. Matuszek, D. R. MacFarlane, A.N. Simonov, Electroreduction of nitrogen with almost 100% current-to-ammonia efficiency, Nature 609 (2022), https://doi.org/10.1038/s41586-022-05108-y.
[10] S.Z. Andersen, V. Čolić, S. Yang, J.A. Schwalbe, A.C. Nielander, J.M. McEnaney, K. Enemark-Rasmussen, J.G. Baker, A.R. Singh, B.A. Rohr, M.J. Statt, S.J. Blair, S. Mezzavilla, J. Kibsgaard, P.C.K. Vesborg, M. Cargnello, S.F. Bent, T.F. Jaramillo, I.E.L. Stephens, J.K. Nørskov, I. Chorkendorff, A rigorous electrochemical ammonia synthesis protocol with quantitative isotope measurements, Nature 570 (2019) 504–508, https://doi.org/10.1038/s41586-019-1260-x.

[11] L. Li, C. Tang, D. Yao, Y. Zheng, S.Z. Qiao, Electrochemical nitrogen reduction: identification and elimination of contamination in electrolyte, ACS Energy Lett.. 4 (2019), https://doi.org/10.1021/acsenergylett.9b01573.

[12] L.F. Greenlee, J.N. Renner, S.L. Foster, The use of controls for consistent and accurate measurements of electrocatalytic ammonia synthesis from Dinitrogen, ACS Catal. 8 (2018), https://doi.org/10.1021/acscatal.8b02120.

[13] S. Wang, W. Wei, X. Lv, B. Huang, Y. Dai, W supported on g-CN manifests high activity and selectivity for N2 electroreduction to NH3, J. Mater. Chem. a Mater. 8 (2020), https://doi.org/10.1039/c9ta10935h.

[14] T. Wu, M.M. Melander, K. Honkala, Coadsorption of NRR and HER intermediates determines the performance of Ru-N4 toward electrocatalytic N2 reduction, ACS Catal. 12 (2022), https://doi.org/10.1021/acscatal.1c05820.

[15] C. Choi, G.H. Gu, J. Noh, H.S. Park, Y. Jung, Understanding potential-dependent competition between electrocatalytic dinitrogen and proton reduction reactions, Nat. Commun. 12 (2021), https://doi.org/10.1038/s41467-021-24539-1.

[16] Z.-J. Zhao, S. Liu, S. Zha, D. Cheng, F. Studt, G. Henkelman, J. Gong, Theory-guided design of catalytic materials using scaling relationships and reactivity descriptors, Nat. Rev. Mater. 4 (2019) 792–804, https://doi.org/10.1038/s41578-019-0152-x.

[17] K.S. Exner, A universal descriptor for the screening of electrode materials for multiple-electron processes: beyond the thermodynamic overpotential, ACS Catal. 10 (2020) 12607–12617, https://doi.org/10.1021/acscatal.0c03865.

[18] E. Skúlason, T. Bligaard, S. Gudmundsdóttir, F. Studt, J. Rossmeisl, F. Abild-Pedersen, T. Vegge, H. Jónsson, J.K. Nørskov, A theoretical evaluation of possible transition metal electro-catalysts for N $_2$ reduction, Phys. Chem. Chem. Phys. 14 (2012) 1235–1245, https://doi.org/10.1039/C1CP22271F.

[19] J.H. Montoya, C. Tsai, A. Vojvodic, J.K. Nørskov, The challenge of electrochemical ammonia synthesis: a new perspective on the role of nitrogen scaling relations, ChemSusChem. 8 (2015) 2180–2186, https://doi.org/10.1002/cssc.201500322.

[20] Y. Guo, G. Wang, S. Shen, G. Wei, G. Xia, J. Zhang, On scaling relations of single atom catalysts for electrochemical ammonia synthesis, Appl. Surf. Sci. 550 (2021) 149283, https://doi.org/10.1016/j.apsusc.2021.149283.

[21] K. Ye, M. Hu, Q.K. Li, Y. Luo, J. Jiang, G. Zhang, Cooperative single-atom active centers for attenuating the linear scaling effect in the nitrogen reduction reaction, J. Phys. Chem. Lett. 12 (2021), https://doi.org/10.1021/acs.jpclett.1c01307.

[22] B.C. Yeo, J. Kong, D. Kim, W.A. Goddard, H.S. Park, S.S. Han, Electronic structural origin of the catalytic activity trend of transition metals for electrochemical nitrogen reduction, J. Phys. Chem. C (2019) 123, https://doi.org/10.1021/acs.jpcc.9b08729.

[23] A. Wang, J. Li, T. Zhang, Heterogeneous single-atom catalysis, Nat. Rev. Chem. 2 (2018) 65–81, https://doi.org/10.1038/s41570-018-0010-1.

[24] F. Kraushofer, G.S. Parkinson, Single-atom catalysis: insights from Model Systems, Chem. Rev. 122 (2022) 14911–14939, https://doi.org/10.1021/acs.chemrev.2c00259.

[25] S.K. Kaiser, Z. Chen, D. Faust Akl, S. Mitchell, J. Pérez-Ramírez, Single-atom catalysts across the periodic table, Chem. Rev. 120 (2020) 11703–11809, https://doi.org/10.1021/acs.chemrev.0c00576.

[26] B. Singh, M.B. Gawande, A.D. Kute, R.S. Varma, P. Fornasiero, P. McNeice, R. V. Jagadeesh, M. Beller, R. Zbořil, Single-atom (Iron-Based) catalysts: synthesis and applications, Chem. Rev. 121 (2021) 13620–13697, https://doi.org/10.1021/acs.chemrev.1c00158.

[27] M.A. Bajada, J. Sanjosé-Orduna, G. Di Liberto, S. Tosoni, G. Pacchioni, T. Noël, G. Vilé, Interfacing single-atom catalysis with continuous-flow organic electrosynthesis, Chem. Soc. Rev. 51 (2022) 3898–3925, https://doi.org/10.1039/D2CS00100D.

[28] S. Razzaq, S. Faridi, S. Kenmoe, M. Usama, D. Singh, L. Meng, F. Vines, F. Illas, K. S. Exner, MXenes spontaneously form active and selective single-atom centers under anodic polarization conditions, J. Am. Chem. Soc. 147 (2025) 161–168, https://doi.org/10.1021/jacs.4c08518.

[29] H. Oschinski, Á. Morales-García, F. Illas, Interaction of first row transition metals with M $_2$ C (M = Ti, Zr, Hf, V, Nb, Ta, Cr, Mo, and W) MXenes: a quest for single-atom catalysts, J. Phys. Chem. C 125 (2021) 2477–2484, https://doi.org/10.1021/acs.jpcc.0c10877.

[30] F. Chen, X. Jiang, L. Zhang, R. Lang, B. Qiao, Single-atom catalysis: bridging the homo- and heterogeneous catalysis, Chin. J. Cataly. 39 (2018) 893–898, https://doi.org/10.1016/S1872-2067(18)63047-5.

[31] Z. Chen, E. Vorobyeva, S. Mitchell, E. Fako, M.A. Ortuño, N. López, S.M. Collins, P. A. Midgley, S. Richard, G. Vilé, J. Pérez-Ramírez, A heterogeneous single-atom palladium catalyst surpassing homogeneous systems for Suzuki coupling, Nat. Nanotechnol. 13 (2018) 702–707, https://doi.org/10.1038/s41565-018-0167-2.

[32] X. Shao, X. Yang, J. Xu, S. Liu, S. Miao, X. Liu, X. Su, H. Duan, Y. Huang, T. Zhang, Iridium single-atom catalyst performing a quasi-homogeneous hydrogenation transformation of CO2 to formate, Chem. 5 (2019) 693–705, https://doi.org/10.1016/j.chempr.2018.12.014.

[33] K. Qian, H. Chen, W. Li, Z. Ao, Y. Wu, X. Guan, Single-atom Fe catalyst outperforms its homogeneous counterpart for activating peroxymonosulfate to achieve effective degradation of organic contaminants, Environ. Sci. Technol. 55 (2021) 7034–7043, https://doi.org/10.1021/acs.est.0c08805.

[34] J. Cho, T. Lim, H. Kim, L. Meng, J. Kim, S. Lee, J.H. Lee, G.Y. Jung, K.-S. Lee, F. Viñes, F. Illas, K.S. Exner, S.H. Joo, C.H. Choi, Importance of broken geometric symmetry of single-atom Pt sites for efficient electrocatalysis, Nat. Commun. 14 (2023) 3233, https://doi.org/10.1038/s41467-023-38964-x.

[35] C. Copéret, M. Chabanas, R.P. Saint-Arroman, J.-M. Basset, Homogeneous and heterogeneous catalysis: bridging the gap through surface organometallic chemistry, Angew. Chemie Int. Ed. 42 (2003) 156–181, https://doi.org/10.1002/anie.200390072.

[36] C. Copéret, A. Comas-Vives, M.P. Conley, D.P. Estes, A. Fedorov, V. Mougel, H. Nagae, F. Núñez-Zarur, P.A. Zhizhko, Surface organometallic and coordination chemistry toward single-site heterogeneous catalysts: strategies, methods, structures, and activities, Chem. Rev. 116 (2016) 323–421, https://doi.org/10.1021/acs.chemrev.5b00373.

[37] Y. Zhang, J. Yang, R. Ge, J. Zhang, J.M. Cairney, Y. Li, M. Zhu, S. Li, W. Li, The effect of coordination environment on the activity and selectivity of single-atom catalysts, Coord. Chem. Rev. 461 (2022) 214493, https://doi.org/10.1016/j.ccr.2022.214493.

[38] X. Li, H. Rong, J. Zhang, D. Wang, Y. Li, Modulating the local coordination environment of single-atom catalysts for enhanced catalytic performance, Nano Res. 13 (2020) 1842–1855, https://doi.org/10.1007/s12274-020-2755-3.

[39] G. Di Liberto, L.A. Cipriano, G. Pacchioni, Single atom catalysts: what matters most, the active site or the surrounding? ChemCatChem 14 (2022) https://doi.org/10.1002/cctc.202200611.

[40] I. Matanovic, K. Artyushkova, M.B. Strand, M.J. Dzara, S. Pylypenko, P. Atanassov, Core level shifts of hydrogenated pyridinic and pyrrolic nitrogen in the nitrogen-containing graphene-based electrocatalysts: in-plane vs edge defects, J. Phys. Chem. C 120 (2016) 29225–29232, https://doi.org/10.1021/acs.jpcc.6b09778.

[41] H. Fei, J. Dong, M.J. Arellano-Jiménez, G. Ye, N.Dong Kim, E.L.G. Samuel, Z. Peng, Z. Zhu, F. Qin, J. Bao, M.J. Yacaman, P.M. Ajayan, D. Chen, J.M. Tour, Atomic cobalt on nitrogen-doped graphene for hydrogen generation, Nat. Commun. 6 (2015) 8668, https://doi.org/10.1038/ncomms9668.

[42] L. Lai, J.R. Potts, D. Zhan, L. Wang, C.K. Poh, C. Tang, H. Gong, Z. Shen, J. Lin, R. S. Ruoff, Exploration of the active center structure of nitrogen-doped graphene-based catalysts for oxygen reduction reaction, Energy Environ. Sci. 5 (2012), https://doi.org/10.1039/c2ee21802j.

[43] Y. Shao, S. Zhang, M.H. Engelhard, G. Li, G. Shao, Y. Wang, J. Liu, I.A. Aksay, Y. Lin, Nitrogen-doped graphene and its electrochemical applications, J. Mater. Chem. 20 (2010), https://doi.org/10.1039/c0jm00782j.

[44] C. Saetta, I. Barlocco, G. Di Liberto, G. Pacchioni, Key ingredients for the screening of single atom catalysts for the hydrogen evolution reaction: the case of titanium nitride, Small (2024), https://doi.org/10.1002/smll.202401058.

[45] G. Di Liberto, G. Pacchioni, Modeling single-atom catalysis, Adv. Mater. (2023), https://doi.org/10.1002/adma.202307150.

[46] J. Wu, Y.X. Yu, Multi-level descriptor construction for screening eligible single-atom-embedded ternary B3C2P3Monolayers as nitrogen fixation catalysts, J. Phys. Chem. C 126 (2022) 12460–12471, https://doi.org/10.1021/acs.jpcc.2c02876.

[47] E. Dai, W. An, R. Guo, X. Shi, Y. Li, Y. Wang, M. Liu, Two-dimensional C2N-based single-atom catalyst with complex microenvironment for enhanced electrochemical nitrogen reduction: a descriptor-based design, J. Energy Chem. 97 (2024) 110–119, https://doi.org/10.1016/j.jechem.2024.05.045.

[48] C. Fang, W. An, Single-metal-atom site with high-spin state embedded in defective BN nanosheet promotes electrocatalytic nitrogen reduction, Nano Res. 14 (2021) 4211–4219, https://doi.org/10.1007/s12274-021-3373-4.

[49] G. Kresse, J. Hafner, Ab initio molecular dynamics for liquid metals, Phys. Rev. B 47 (1993) 558–561, https://doi.org/10.1103/PhysRevB.47.558.

[50] G. Kresse, J. Hafner, Ab initio molecular-dynamics simulation of the liquid-metal–amorphous-semiconductor transition in germanium, Phys. Rev. B 49 (1994) 14251–14269, https://doi.org/10.1103/PhysRevB.49.14251.

[51] G. Kresse, J. Furthmüller, Efficiency of ab-initio total energy calculations for metals and semiconductors using a plane-wave basis set, Comput. Mater. Sci. 6 (1996) 15–50, https://doi.org/10.1016/0927-0256(96)00008-0.

[52] J.P. Perdew, K. Burke, M. Ernzerhof, Generalized gradient approximation made simple, Phys. Rev. Lett. 77 (1996) 3865–3868, https://doi.org/10.1103/PhysRevLett.77.3865.

[53] P.E. Blöchl, Projector augmented-wave method, Phys. Rev. B 50 (1994) 17953–17979, https://doi.org/10.1103/PhysRevB.50.17953.

[54] G. Kresse, D. Joubert, From ultrasoft pseudopotentials to the projector augmented-wave method, Phys. Rev. B 59 (1999) 1758–1775, https://doi.org/10.1103/PhysRevB.59.1758.

[55] H.J. Monkhorst, J.D. Pack, Special Points Brillonin-Zone Integ.* (1976).

[56] S. Grimme, J. Antony, S. Ehrlich, H. Krieg, A consistent and accurate ab initio parametrization of density functional dispersion correction (DFT-D) for the 94 elements H-Pu, J. Chem. Phys. 132 (2010) 154104, https://doi.org/10.1063/1.3382344.

[57] M.T. Greiner, T.E. Jones, S. Beeg, L. Zwiener, M. Scherzer, F. Girgsdies, S. Piccinin, M. Armbrüster, A. Knop-Gericke, R. Schlögl, Free-atom-like d states in single-atom alloy catalysts, Nat. Chem. 10 (2018) 1008–1015, https://doi.org/10.1038/s41557-018-0125-5.

[58] A.M. Patel, S. Ringe, S. Siahrostami, M. Bajdich, J.K. Nørskov, A.R. Kulkarni, Theoretical approaches to describing the oxygen reduction reaction activity of single-atom catalysts, J. Phys. Chem. C 122 (2018) 29307–29318, https://doi.org/10.1021/acs.jpcc.8b09430.

[59] G. Di Liberto, L.A. Cipriano, G. Pacchioni, Universal principles for the rational design of single atom electrocatalysts? Handle with care, ACS Catal. (2022) 5846–5856, https://doi.org/10.1021/acscatal.2c01011.

[60] I. Barlocco, L.A. Cipriano, G. Di Liberto, G. Pacchioni, Modeling hydrogen and oxygen evolution reactions on single atom catalysts with density functional theory: role of the functional, Adv. Theory Simul. (2022) 2200513, https://doi.org/10.1002/adts.202200513.

[61] D. Misra, G. Di Liberto, G. Pacchioni, CO2 Electroreduction on single atom catalysts: role of the DFT functional, Phys. Chem. Chem. Phys. (2024), https://doi.org/10.1039/D4CP00175C.

[62] A.M. Patel, S. Ringe, S. Siahrostami, M. Bajdich, J.K. Nørskov, A.R. Kulkarni, Theoretical approaches to describing the oxygen reduction reaction activity of

single-atom catalysts, J. Phys. Chem. C 122 (2018) 29307–29318, https://doi.org/10.1021/acs.jpcc.8b09430.
[63] C. Adamo, V. Barone, Toward reliable density functional methods without adjustable parameters: the PBE0 model, J. Chem. Phys. 110 (1999) 6158–6170, https://doi.org/10.1063/1.478522.
[64] J.K. Nørskov, T. Bligaard, A. Logadottir, J.R. Kitchin, J.G. Chen, S. Pandelov, U. Stimming, Trends in the exchange current for hydrogen evolution, J. Electrochem. Soc. 152 (2005), https://doi.org/10.1149/1.1856988. J23.
[65] J.K. Nørskov, J. Rossmeisl, A. Logadottir, L. Lindqvist, J.R. Kitchin, T. Bligaard, H. Jónsson, Origin of the overpotential for oxygen reduction at a fuel-cell cathode, J. Phys. Chem. B 108 (2004) 17886–17892, https://doi.org/10.1021/jp047349j.
[66] E. Di Simone, G. Vilé, G. Di Liberto, G. Pacchioni, Decoding the role of adsorbates entropy in the reactivity of single-atom catalysts, ACS Catal. 15 (2025) 447–456, https://doi.org/10.1021/acscatal.4c04472.
[67] D. Misra, G. Di Liberto, G. Pacchioni, CO2 electroreduction on single atom catalysts: is water just a solvent? J. Catal. 422 (2023) 1–11, https://doi.org/10.1016/j.jcat.2023.04.002.
[68] G. Ertl, Primary steps in catalytic synthesis of ammonia, J. Vacuum Sci. Technol. A: Vacuum, Surf., Films 1 (1983), https://doi.org/10.1116/1.572299.
[69] L. Meng, F. Viñes, F. Illas, Unveiling the synergy between surface terminations and boron configuration in boron-based Ti $_3$ C $_2$ MXenes electrocatalysts for nitrogen reduction reaction, ACS Catal. 14 (2024) 15429–15443, https://doi.org/10.1021/acscatal.4c03415.
[70] L. Zhong, S. Li, Unconventional oxygen reduction reaction mechanism and scaling relation on single-atom catalysts, ACS Catal. 10 (2020) 4313–4318, https://doi.org/10.1021/acscatal.0c00815.
[71] I. Barlocco, L.A. Cipriano, G. Di Liberto, G. Pacchioni, Does the Oxygen Evolution Reaction follow the classical OH*, O*, OOH* path on single atom catalysts? J. Catal. 417 (2023) 351–359, https://doi.org/10.1016/j.jcat.2022.12.014.
[72] J. Wu, J.H. Li, Y.X. Yu, Single Nb or W atom-embedded BP monolayers as highly selective and stable electrocatalysts for nitrogen fixation with low-onset potentials, ACS Appl. Mater. Interf. 13 (2021) 10026–10036, https://doi.org/10.1021/acsami.0c21429.
[73] R.F. Bader, Atoms in molecules, Acc. Chem. Res. 18 (1) (1985) 9–15.
[74] A. Walsh, A.A. Sokol, J. Buckeridge, D.O. Scanlon, C.R.A. Catlow, Electron counting in solids: oxidation states, partial charges, and ionicity, J. Phys. Chem. Lett. 8 (2017) 2074–2075, https://doi.org/10.1021/acs.jpclett.7b00809.
[75] R. Guo, W. An, M. Liu, Y. Li, Y. Wang, S. Yang, Y. Men, J. Wang, S. Liu, Modulating the coordination environment of active site structure for enhanced electrochemical nitrogen reduction: the mechanistic insight and an effective descriptor, Appl. Surf. Sci. 644 (2024), https://doi.org/10.1016/j.apsusc.2023.158799.
[76] I. Barlocco, M. Spotti, G. Di Liberto, G. Pacchioni, Electrochemical nitrogen reduction reaction from Ab Initio thermodynamics: single versus dual atom catalysts, Adv. Theory Simul. (2024), https://doi.org/10.1002/adts.202400536.
[77] T. Pu, J. Ding, F. Zhang, K. Wang, N. Cao, E.J.M. Hensen, P. Xie, Dual atom catalysts for energy and environmental applications, Angew. Chemie - Int. Ed. 62 (2023), https://doi.org/10.1002/anie.202305964.
[78] R. Li, D. Wang, Superiority of dual-atom catalysts in electrocatalysis: one step further than single-atom catalysts, Adv. Energy Mater. 12 (2022), https://doi.org/10.1002/aenm.202103564.
[79] H. Niu, X. Wang, C. Shao, Z. Zhang, Y. Guo, Computational screening single-atom catalysts supported on g-CN for N2 reduction: high activity and selectivity, ACS Sustain. Chem. Eng. 8 (2020) 13749–13758, https://doi.org/10.1021/ACSSUSCHEMENG.0C04401.
[80] Z. Chen, J. Zhao, C.R. Cabrera, Z. Chen, Computational screening of efficient single-atom catalysts based on graphitic carbon nitride (g-C 3 N 4) for nitrogen electroreduction, Small Methods 3 (2019) 1800368, https://doi.org/10.1002/smtd.201800368.
[81] I. Barlocco, G. Di Liberto, G. Pacchioni, New scaling relationships for the oxygen evolution reaction on single atom catalysts, Catal. Today 427 (2024) 114409, https://doi.org/10.1016/j.cattod.2023.114409.
[82] K.S. Exner, A universal descriptor for the screening of electrode materials for multiple-electron processes: beyond the thermodynamic overpotential, ACS Catal. 10 (2020) 12607–12617, https://doi.org/10.1021/acscatal.0c03865.
[83] Y.X. Yu, Oxygen-transfer from N2O to CO via Y-doped Ti2CO2 (MXene) monolayer at room temperature: density functional theory and ab initio molecular simulation studies, J. Colloid. Interf. Sci. 695 (2025), https://doi.org/10.1016/j.jcis.2025.137799.
[84] D. Singh, S. Razzaq, E. Tayyebi, K.S. Exner, Selectivity control in the nitrogen reduction reaction over Mo $_2$ C MXene by a nitrogen-rich environment, ACS Catal. 15 (2025) 5589–5600, https://doi.org/10.1021/acscatal.4c04878.
[85] E. Tayyebi, K.S. Exner, Understanding free-energy landscapes in electrocatalysis: a case study on nitrate reduction over Au(111), ACS Electrochem. 1 (2025) 910–920, https://doi.org/10.1021/acselectrochem.4c00210.
[86] K.S. Exner, On the optimization of nitrogen-reduction electrocatalysts: breaking scaling relation or catalytic resonance theory? ChemCatChem 14 (2022) https://doi.org/10.1002/cctc.202200366.
[87] M. Usama, S. Razzaq, K.S. Exner, Design criteria for active and selective catalysts in the nitrogen oxidation reaction, ACS Phys. Chem. Au 5 (2025) 38–46, https://doi.org/10.1021/acsphyschemau.4c00058.